24th INTERNATIONAL CONGRESS ON SOUND AND VIBRATION
23–27 July 2017, London

LONGITUDINAL VIBRATION AND UNSTEADY THRUST TRANSMISSION OF THE RIM DRIVEN THRUSTER INDUCED BY INGESTED TURBULENCE

Yong Chen*, Feng Chen, X. H Long

Shanghai Jiao Tong University, State Key Laboratory of Mechanical system and vibration, 800 Dong Chuan Road, Shanghai, P.R. China.

email: chenyong@sjtu.edu.cn

The longitudinal vibration characteristics of the rim driven thruster (RDT) induced by the ingested turbulence are numerically studied and compared with that of traditional shaft driven propeller (SDP). The pressure spectrum acted on the blade surface is firstly computed using the correlation method based on the strip theory and the statistical characteristics of isotropic turbulence. Applied the computed pressure spectrum as excitation, the random vibration response of the whole immersed thruster can be obtained by mode superposition method. The differences between the vibration responses, especially the unsteady thrust transmission characteristics, of the two kinds of propulsors that have the same blade geometry are discussed. The computational results show that RDT has relatively lower hydrodynamic damping in the lower bending modes, but its amplification effect on the unsteady thrust is still distinctly lower than that of SDP because it subjects to lower modal excitation force. A potential merit of traditional SDP is that it has more prominent attenuation effect on the unsteady thrust in the frequency band between the first and second bending mode of blades.

Keywords: Rim driven thruster; Ingested turbulence; Vibration; Unsteady thrust

1. Introduction

The fluctuating forces at propeller are an important cause of sound radiation from a submarine in the low frequency range [1]. These unsteady forces consist of periodic force components and broadband force components [2, 3]. The periodic force components often occur at multiples of the blade passage frequency and are considered to the result from the unsteady pressure distribution on the propeller blades[4, 5]. The broadband force components often distribute from several to several hundred hertz, with some 'hump' around the first and second blade rate frequencies [6, 7]. Among which, the low frequency broadband forces are mainly due to the interaction of the inflow turbulence with the propeller blades. The turbulence is generated by the boundary layer of hull and all the appendages upstream of the propeller, superposed on the ambient free-stream turbulence.

Compared with the traditional shaft driven propeller (SDP), the electric rim driven thruster (RDT) is a relatively new marine propulsor that has been developed in recent years. It uses a permanent magnet rotor built into a rim around the propeller [8]. The permanent magnetic rotor is embedded in a rim around the tips of the blade as shown in Figure 1(a). The motor stator is mounted in the duct. RDT has shown lots of advantages compared with SDP, such as less energy loss due to the vanish of gap between blade and duct, more flexible installation due to the modular design and more prompt steering [9-11]. But as a potential propulsor for the future ship, its vibration and acoustic characteristics have seldom been studied. As can be seen, there is great difference between the blade configuration of the RDT and traditional SDP. How does the blade configuration influences the total unsteady thrust transmission is worth studying. In this paper, the multimodal vibration response caused by the

ingested turbulence induced broadband excitation of RDT is numerically investigated. Meanwhile, the response a corresponding SDP with the similar blade geometry is computed too. Our motivation is to explore the possible stealth capability of RDT by comparing it with traditional SDP.

2. Theoretical approach

In order to calculate the characteristics of the fluctuating force over the blade surfaces, the blade is divided into a number of strip elements along its radius. The time-dependent forces acting on various strip elements are related by virtue of spatial and temporal correlation of the velocity fluctuations in the approach stream as well as by virtue of the induced effects that take place between adjacent elements. In the following tensor equations, subscripts are used to denote the direction along the coordinate axes, while superscripts are used to denote the blade element involved. For example, $F_{ij}^{\alpha\beta}(t,\tau)$ denotes the hydrodynamic force acting on the α-th element in the direction i at the instant of time t caused by a velocity fluctuation of unit magnitude in the direction j on of the β-th element at the instant τ. With this convention, the hydrodynamic force acting on the α-th element at time t in the direction i, $l_i^{\alpha}(t)$ due to the influence of velocity fluctuation at all elements β, and in all the direction j, over all time τ, is expressed as

$$l_i^{\alpha}(t)=\int_{-\infty}^{t}F_{ij}^{\alpha\beta}(t,\tau)u_j^{\beta}(\tau)d\tau \quad \text{where } i,j=1,2,3 \quad \alpha,\beta=1,2,...\text{n} \tag{1}$$

Since l_i^{α} is a random function of time in a turbulent flow, a statistical approach must be employed. If the inflow turbulence is time-invariant, the correlation function of unsteady forces, $\Phi_{ij}^{\alpha\beta}$ becomes

$$\begin{aligned}\Phi_{ij}^{\alpha\beta}(\tau)&=E\left[l_i^{\alpha}(t)l_j^{\beta}(t+\tau)\right]\\&=\lim_{T\to\infty}\frac{1}{T}\int_0^T\int_0^{\infty}\int_0^{\infty}F_{ik}^{\alpha\gamma}(\tau_1)F_{jm}^{\beta\delta}(\tau_2)u_k^{\gamma}(t-\tau_1)u_m^{\delta}(t+\tau-\tau_2)d\tau_1d\tau_2dt\\&=\int_0^{\infty}\int_0^{\infty}F_{ik}^{\alpha\gamma}(\tau_1)F_{jm}^{\beta\delta}(\tau_2)R_{km}^{\gamma\delta}(t+\tau-\tau_2)d\tau_1d\tau_2\end{aligned} \tag{2}$$

where $R_{km}^{\gamma\delta}$ is the velocity correlation function between fluid point in the turbulence

$$R_{km}^{\gamma\delta}(t+\tau-\tau_2)=\lim_{T\to\infty}\frac{1}{T}\int_0^{\infty}u_k^{\gamma}(t-\tau_1)u_m^{\delta}(t+\tau-\tau_2)dt \tag{3}$$

The corresponding frequency spectrum of the correlated force fluctuations of the α-th element in the direction i due to the β-th element in the direction j can be found by taking the Fourier transform of the above correlation tensor:

$$\begin{aligned}\Psi_{l_il_t}^{\alpha\beta}(\omega)&=\frac{1}{2\pi}\int_{-\infty}^{\infty}\Phi_{ij}^{\alpha\beta}(\tau)d\tau=\frac{1}{2\pi}\int_0^T\int_0^{\infty}\int_0^{\infty}F_{ik}^{\alpha\gamma}(\tau_1)d\tau_1F_{jm}^{\beta\delta}(\tau_2)d\tau_2R_{km}^{\gamma\delta}(t+\tau-\tau_2)d\tau\\&=\left[H_{ik}^{\alpha\gamma}(\omega)\right]^{*}\left[H_{jm}^{\beta\gamma}(\omega)\right]G_{km}^{\gamma\delta}(\omega)\end{aligned} \tag{4}$$

where $H_{ik}^{\alpha\beta}(\omega)$ is the hydrodynamic frequency response function and $G_{km}^{\gamma\delta}(\omega)$ is the Fourier transform of the velocity correlation function. Once the unsteady forces due to inflow turbulence is computed, the force spectrum between each strip of the propeller blade is also determined and can be fed into the random vibration analysis program of the propeller.

The solution for a one-dimensional turbulent field yields the standard two-dimensional Sears function [5, 13], which relates the lift per unit span to the incident downwash amplitude

$$dL(k_1)/dy_3=\pi\rho_0CU_{\infty}\tilde{u}_2(k_1,\omega)\xi(k_1C/2)e^{-i\omega t} \tag{5}$$

where $k_1C/2=\omega C/2U_{\infty}$. The Sears function gives the amplitude and phase [5, 14](relative to the disturbance at the mid-chord)

$$\xi(k_1C/2)=\frac{(2i/\pi)(2/k_1C)}{H_1^{(2)}(k_1C/2)+iH_0^{(2)}(k_1C/2)} \tag{6}$$

where $H_1^{(2)}$ and $H_0^{(2)}$ are cylindrical Hankel functions. The pressure difference between the upper and lower surfaces has been given by a number of investigators in the form [13]

$$\Delta p = 2\rho_0 U_\infty \tilde{u}_2\left(\mathrm{k}_1, \mathrm{k}_3\,\omega\right)\sqrt{\frac{C/2-y_1}{C/2+y_1}}\,\ell_{2D}\left(k_1 C, k_3 C\right)e^{+i(k_3 y_3-\omega t)} \tag{7}$$

The turbulent inflow where the practical thruster operates is very complex. But in this paper we assume that the two point velocity correlations are invariant with translations in position, or in other words, a spatially homogeneous turbulent flow. These assumptions allow the velocity correlations between any two points to be written in terms of scalar longitudinal and transverse normalized auto-correlation functions. With additional assumptions of a divergence-free flow field and exponentially decaying normalized stream-wise velocity correlation function, given as $f(\eta)=e^{-\eta/\Lambda}$, the velocity correlation tensor takes the following form given by Hinze [15]

$$R_{ij} = u^2\left[\frac{1}{2r\Lambda}r_i r_j + \left(1-\frac{r}{2\Lambda}\right)\delta_{ij}\right]e^{-\frac{r(\tau)}{\Lambda}} \tag{8}$$

For blades rotating in a turbulent field with rotational speed Ω, $r(\tau)$ is

$$r(\tau) = \sqrt{(dx)^2 + r_\alpha^2 + r_\beta^2 - 2r_\alpha r_\beta\left(\theta_\alpha(0)-\theta_\beta(0)+\Omega\tau\right)} \tag{9}$$

Let the mean inflow to the propeller be denoted by $\bar{u}^\alpha$, then the unsteady angle of attack becomes

$$\alpha(\tau) = \tan^{-1}\frac{u_N^\alpha}{\bar{u}^\alpha} \approx \frac{u_N^\alpha}{\bar{u}^\alpha} \tag{10}$$

with $u_N^\alpha = u_x^\alpha\cos\phi_\alpha + u_\theta^\alpha\sin\phi_\alpha$. Based on the above definition of R_{NN}, correlation functions are numerically evaluated at given ω values as

$$G_{NN}^{\gamma\delta}(\omega) = \frac{1}{2\pi}\int_{-\infty}^{\infty} R_{NN}^{\gamma\delta}(\tau)e^{-i\omega\tau}d\tau \tag{11}$$

$$\psi_{l_x l_x}^{\alpha\beta}(\omega) = \left[H_{xx}^{\alpha\gamma}(\omega)\right]^*\left[H_{xx}^{\beta\delta}(\omega)\right]G_{NN}^{\gamma\delta}(\omega) \tag{12}$$

Considering the complex geometry of marine propeller, the finite element method is used to compute the random response of the immersed propulsor. Accounting for the fluid around, the discrete linear dynamic system has the equilibrium equation

$$\begin{bmatrix} K_s & S_{fs}^T \\ 0 & K_f \end{bmatrix}\begin{Bmatrix} u(\omega) \\ p(\omega) \end{Bmatrix} + i\omega\begin{bmatrix} C_s & 0 \\ 0 & C_f \end{bmatrix}\begin{Bmatrix} \dot{u}(\omega) \\ \dot{p}(\omega) \end{Bmatrix} - \omega^2\begin{bmatrix} M_s & 0 \\ -S_{fs} & M_f \end{bmatrix}\begin{Bmatrix} \ddot{u}(\omega) \\ \ddot{p}(\omega) \end{Bmatrix} = \begin{bmatrix} F_f(\omega) & 0 \\ 0 & P_s(\omega) \end{bmatrix} \tag{13}$$

where $u(\omega)$ is structure displacement and $p(\omega)$ is the pressure of the fluid (as acoustic element). M_s, K_s C_s are the mass matrix, stiffness matrix and damping matrix of the structure. $F_f(\omega)$ is the external loads exerted on the structure. It is a matrix when the random loading is considered. M_f, K_f and C_f is the coefficient matrix related to the fluid. S_{fs} is the coupling item related to the fluid and structure.

3. 3 Results and discussions

3.1 3.1 Thruster geometry and excitation spectrum

The geometry of the analyzed RDT is shown in the left of the Figure 1. The thruster has ten equally spaced blades with the outer diameter being 2031.9 mm. It is so designed that it is can be conveniently compared with an equivalent propeller. The corresponding propeller with the same blade configuration is shown in the right of Figure 1. The propeller is a 10 scaled version of the propeller that has been studied by Sevik [6] in 1970s. The prototype has a constant chord of 254.2 mm along the span with no skew and square tips. A schematic of the rotor as well as profiles of the blade at its tip and root can be seen in Figure 1. The blade pitch angle measured from the plane of the rotor varies non-linearly from the root to the tip as indicated in [6]. The rotors operate at a design advance ratio of 1.19. The material of propeller blade is set as common steel with $E_p = 210e9\ Pa$ and the stiffness of thrust bearing is set as $k_s = 7.66e7\ N\cdot m$. The material of the rim and the shaft is artificially increased

in order to reduce the influence of the boundary and guarantee that the comparison between two propulsors is reasonable.

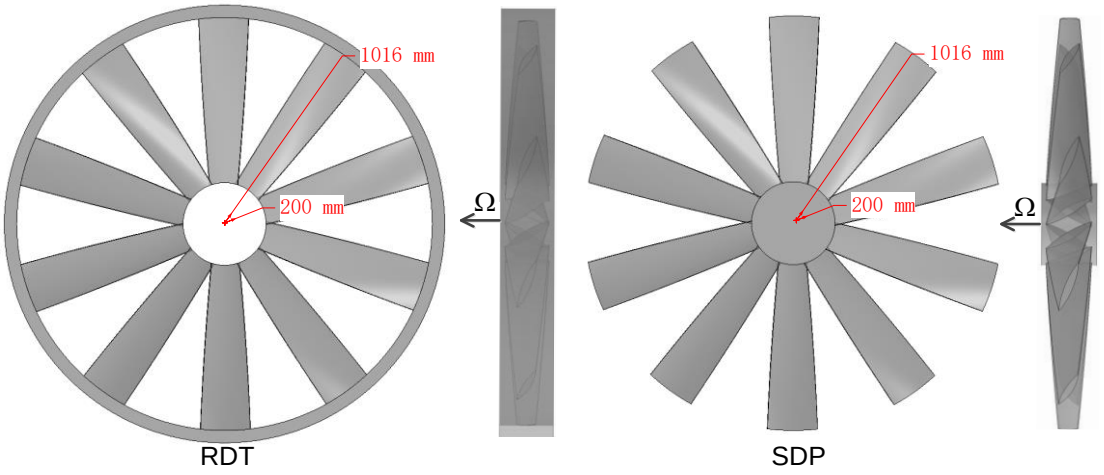

Figure 1 The geometry and dimensions of the analyzed RDT (a) and SDP (b)

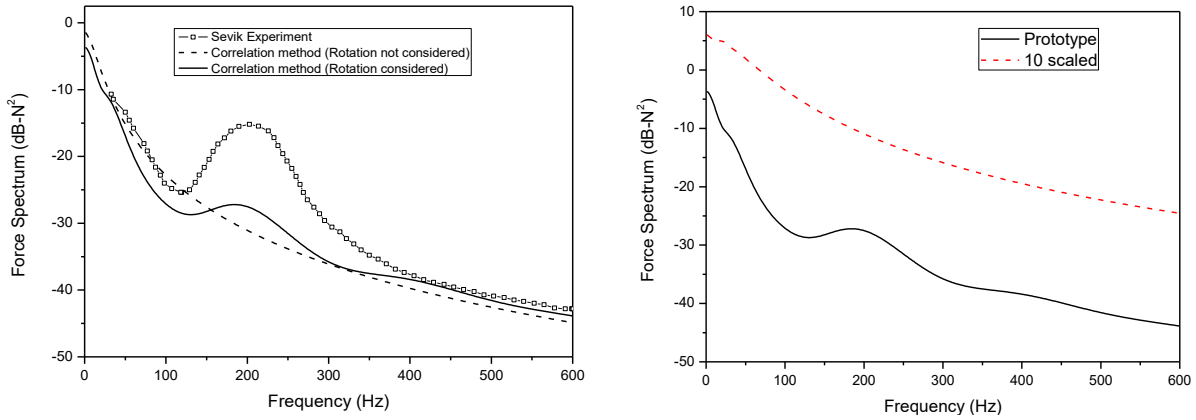

Figure 2 (a) Comparison of correlation method with experiment; (b) Force spectrum comparison of 10 scaled propeller and its proptotype with the same advance ratio and ingested turbulence condition

Sevik's experiment [6] is used to demonstrates the accuracy of the correlation method. The experiment was conducted in the 1.22 m diameter water tunnel. The propeller has ten blades with constant chord length of 25.4 mm and a radius of 101.6 mm. The tunnel speed equals 4.56 m/s and the advance ratio was 1.22. The turbulence level is about 3% with integral length scale being 4 cm. Power spectral density of the propeller thrust is compared in Figure 2(a). Good agreement can be achieved with the theoretical method except that measured spectra shows more significant humps at the first blade frequency. It is perhaps because that the isotropic turbulence hypothesis is not entirely consistent with the practical inflow characteristics. In Figure 2(b), the thrust spectrum of the 10-scaled version propeller is compared with that of the prototype. As a comparison, the inflow condition and the advance ratio is the same for both propeller. The hump occurs about 19Hz for the 10-scaled propeller.

Figure 3 gives the frequencies and corresponding modal shapes of the lowest fifty-one modes of the RDT and SDP. The modal frequency distribution of both models is almost the same. The corresponding modal shapes of the two models are similar too, except the deformation direction. These results guarantee that the following comparison is meaningful. For both models, the first mode at $f_0 = 19Hz$ is the longitudinal rigid motion of rotor with the rim (shaft) mass. The elastic deformation of the propeller itself is not prominent. The subsequent modes occur in groups. In each group, ten

modes almost have the same frequency. It is attributed to the blade cycle-symmetry of the both propulsors. In group 1 at $f_{b1} \approx 38\,Hz$, the mode shape is the first bending mode of cantilever blade. In group 2 at $f_{b2} = 175\,Hz$, the one-node bending mode occurs. The pure torsional mode occurs at $f_t \approx 286\,Hz$ in group 3. In group 4 and 5, two-node and three-node bending modes occur at $f_{b3} = 310\,Hz$ and $f_{b4} = 610\,Hz$ respectively.

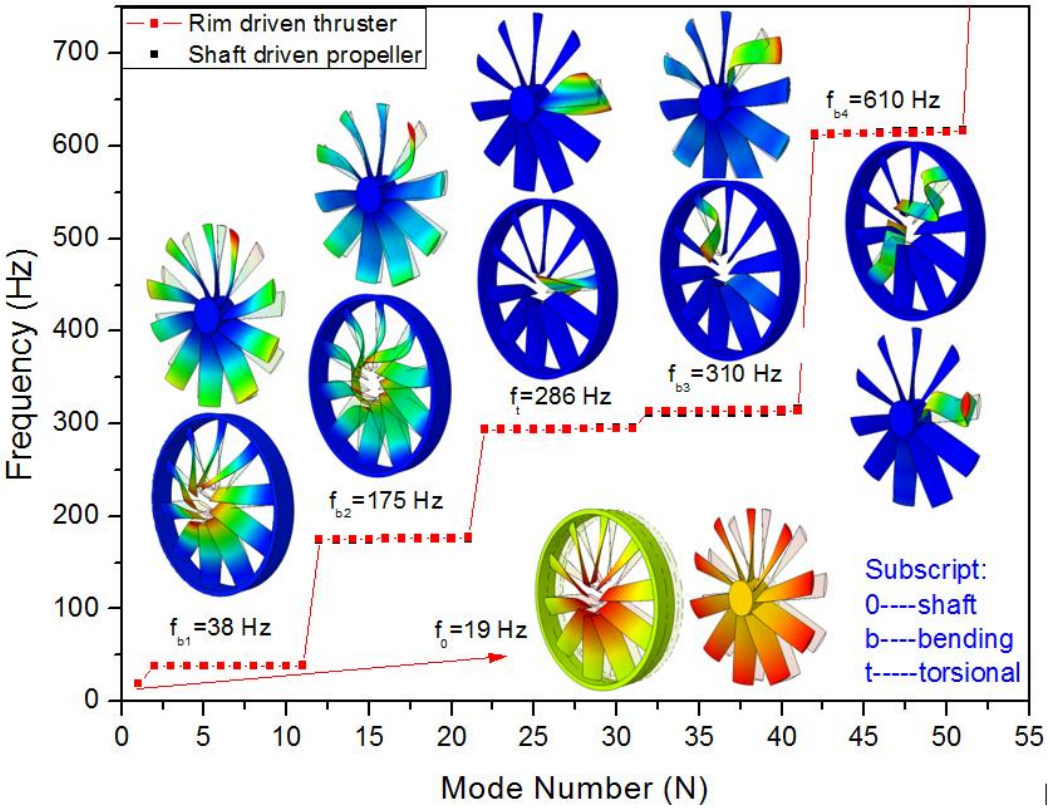

Figure 3 The mode frequencies and mode shapes of the propeller-shaft system

3.2 The random response characteristics of RDT

A typical case is firstly computed when considering the elasticity of both thruster and bearing with $f_0 = 19\,Hz$ and $f_{b1} = 38\,Hz$. The analyzing frequency is ranged from 1 Hz to 350 Hz with 51 orders of modes being considered. In order to understand the response mechanism of the whole thruster, the vibration spectrum at three typical locations on the thruster is extracted and plotted in Figure 4. The locations of the three points are marked in a contour. In general, the amplification effect of the elastic thruster can be distinctly observed in both the rim and the blade except the torsional modes around f_t. The contour on the root mean square of the velocity on the whole thruster within 350 Hz is also shown in Figure 4 but the detailed discussion will be made in the next section. The vibration level at blade tip is distinctly higher than that at the rim except at frequency f_0. At this frequency, the vibration level on the whole disk is almost the same as the vibration level is mainly controlled by the system response of the whole rim and bearing. The discrepancy between Tip1 and Tip2 should be attributed to the torsional vibration of the propeller blades.

Figure 5 compares the transmitted thrust spectrum when both the elasticity of thruster and bearing is considered or not. Three cases have been considered: rigid thruster and bearing with $f_{b1} \to \infty,\ f_0 \to \infty$, elastic thruster and rigid bearing $f_{b1} \to 38\,Hz,\ f_0 \to \infty$, elastic thruster and elastic bearing $f_{b1} \to 38\,Hz,\ f_0 \to 19\,Hz$. It can be seen that the force transmitted to the foundation can be greatly changed by the system elasticity. Firstly, when only the elasticity of the thruster itself is considered, the unsteady thrust almost has the same level with the rigid case except the amplification effect of bending modes and the attenuation effect between two neighboring natural frequencies. But when the

elasticity of bearing is considered, the unsteady thrust is greatly attenuated for the filtering effect of the global mode at f_0. At this condition, the resonance response of the global mode of the thruster-bearing system at f_0 is very prominent. The high amplitude of the response is attributed to the low damping of the bearing (only mechanical damping) and high excitation force in the low frequency band. Totally speaking, both the elasticity of thruster and the thrust bearing need to be considered when we compute the practical thrust spectrum acted on the foundation.

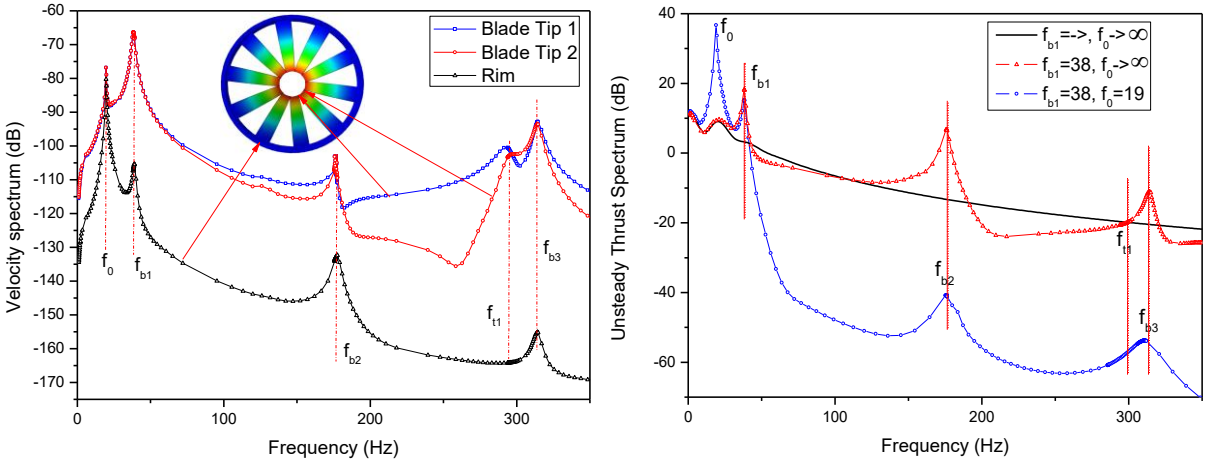

Figure 4 The velocity spectrum at the blade tip and the center of hub with $f_s = 19$ and $f_{b1} = 38\ Hz$

Figure 5 The transmitted unsteady thurst spectrum for three different cases

3.3 3.3 Comparison between two kinds of thrusters

As a comparison, the vibration response of the corresponding SDP is also computed using the same excitation. As stated in section 3.2, there is great difference between the modal shape and the modal damping (mainly the hydrodynamic damping) of the two kinds of thrusters. Two factors can be investigated respectively. Firstly, the influence of modal force is studied by neglecting the hydro-dynamic damping while keep only mechanical and radiation damping. Therefore, the corresponding loss factors of both models are the same in each mode. For the purpose of comparison, the influence of the bearing stiffness is ruled out by setting $f_0 \to \infty$. The vibration spectrum of both kinds of pro-pulsors when all the damping mechanisms are considered is compared in Figure 6(a) and (b). This time, the difference between the RDT and SDP is greatly reduced for the loss factor in the lower modes of SDP is much higher than that RDT as indicated in Figure 6 (b). But still, the response of RDT is smaller than that of SDP, though the difference is greatly discounted.

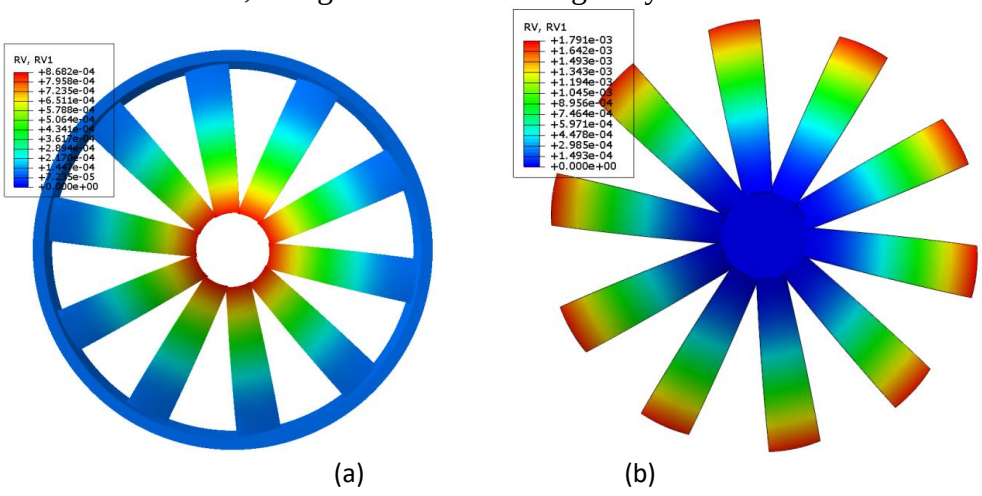

Figure 6 The concour on the root mean square value of velocity (integrated from 1 Hz to 350 Hz) of (a) RDT and (b) SDP with the hydrodanymic damping being considered: $f_0 \to \infty$ and $f_{b1} = 38\ Hz$

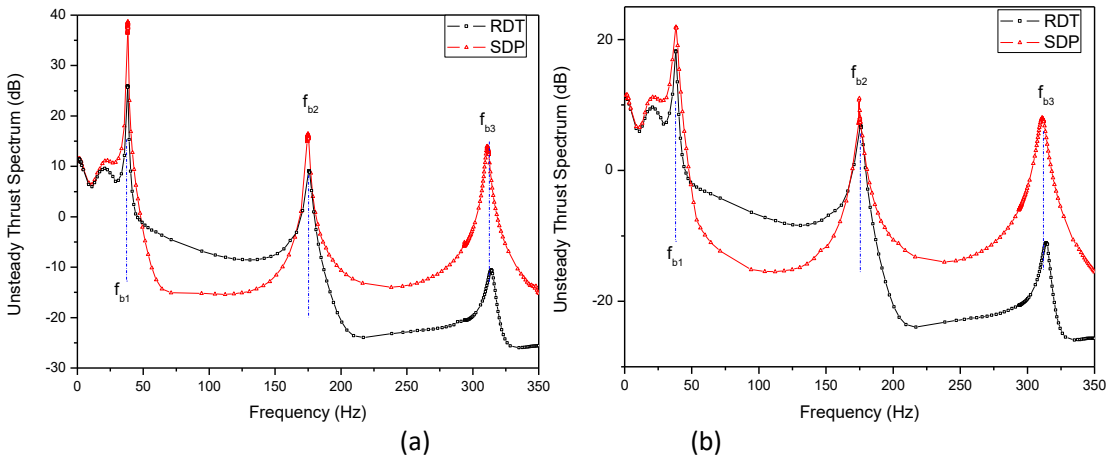

Figure 7 The transmitted unseady thrust comparison between the RDT and SDP when (a) the hydrodynamic damping is not considered and (b) the hydrodynamic damping is considered: $f_0 \to \infty$ and $f_{b1} = 38\ Hz$

The transmitted unsteady thrust for two different cases are compared in Figure 7(a) and (b). When the hydrodynamic damping is neglected, the amplification effect of the SDP is greatly higher. The difference can reach about 15 dB at the first bending frequency f_{b1} and 20 dB at the third bending frequency f_{b3}. But when the hydrodynamic damping is considered, the difference of at the first bending frequency f_{b1} is greatly reduced, though the thrust of the SDP is still higher than that of RDT. On the other hand, the difference at the third bending frequency f_{b3} is nearly not changed. This should be attributed to the low hydrodynamic damping in the high frequency band. Therefore, the resonance response at these frequencies is manly controlled by the mechanical damping, not by the hydrodynamic damping. A merit of traditional SDP can be found is that is has better attenuation effect than RDT in the frequency band between f_{b1} and f_{b2}.

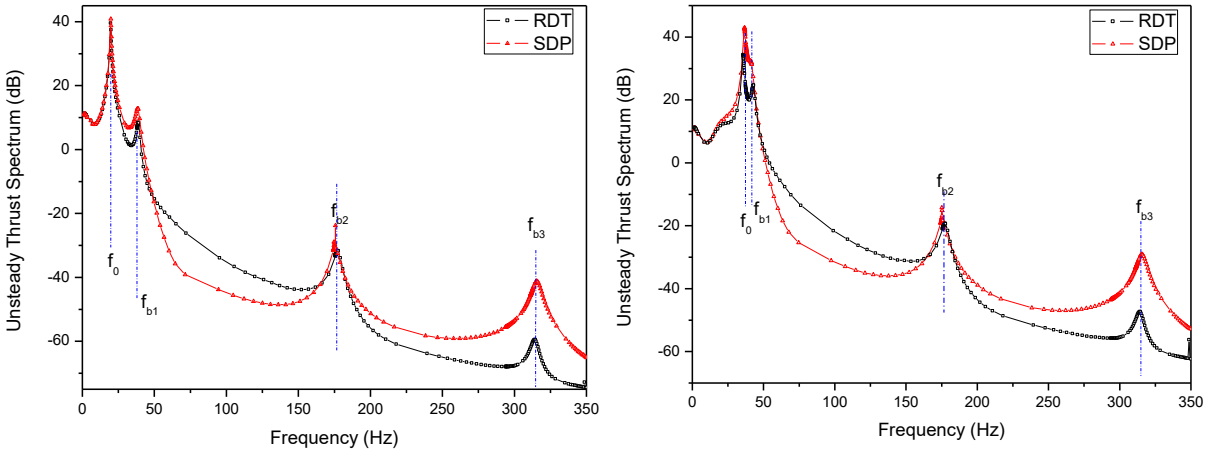

Figure 8 The transmitted unseady thrust comparison between the RDT and SDP with $f_0 = 19\ Hz$ and $f_{b1} = 38\ Hz$; Figure 9 The transmitted unseady thrust comparison between the RDT and SDP with $f_0 \approx 38\ Hz$ and $f_{b1} \approx 38\ Hz$

The unsteady thrust transmission characteristics of the two types of thrusters are also compared when both the elasticity of blade and the bearing are considered. Three typical cases are analyzed with $f_0 = 19\ Hz$, $f_0 = 38\ Hz$ and $f_0 = 57\ Hz$ while keeping $f_{b1} = 38\ Hz$. Figure 8 compares the unsteady thrust transmitted to the foundation when $f_0 = 19\ Hz$. Under the condition $f_0 < f_{b1}$, the base line of the transmitted thrust spectrum is mainly determined by the global mode of the thruster-bearing system

at f_0. The resonance response of SDP at the natural frequencies of the rotor itself is still higher than that of RDT, though the responses of both thruster have been filtered. ; Figure 9 compares the responses of the two types of thruster when both f_0 and f_{b1} approaches 38Hz. In fact, the completely equal cannot be achieved because of the coupling between the two modes. As can be seen, the resonance response induced by the mutually reinforcing of SDP is very distinct. The resonse peak of the RDT is 6dB lower than that of SDP.

4. Conclusion

The elastic vibration characteristics of a ten-bladed rim driven thruster induced by the ingested turbulence are numerically investigated and compared with a traditional shaft driven propeller which has the same blade configuration. The longitudinal vibration and the unsteady thrust transmission characteristics of both types of thruster are compared. The following conclusions can be drawn: (i) Both the bending modes and the torsional mode of the blade are responsive to the random loads induced by the inflow turbulence, but only the bending modes (especially the first order) can amplify the transmitted thrust; (ii) Compared with the traditional SDP, the vibration response of RDT is much lower for the poor coincidence between its modal shape with the spatial distribution of the random loads; (iii) The hydrodynamic loss factor of the RDT of the lower mode, especially the first cantilever beam mode, is much lower than that of the SDP. (iv) When f_0 approaches f_{b1}, the resonance response of RDT is much lower than that of SDP.

REFERENCES

1 D. Ross, Mechanics of Underwater Noise, Penninsula Publishing, Los Altos, 1987.
2 W.K. Blake, Mechanics of Flow-induced Sound and Vibration: Complex flow-structure interactions, Academic Press, 1986.
3 G.F. Homicz, A.R. George, broadband and discrete frequency radiation from subsonic rotors, Journal of sound and vibration, 36 (1974) 23.
4 D.E. Tompson, Propeller time-dependent forces due to non-uniform flow, in, The Pennsylvania State University, 1976.
5 M. Massaro, J.M.R. Graham, The effect of three-dimensionality on the aerodynamic admittance of thin sections in free stream turbulence, Journal of Fluids and Structures, 57 (2015) 10.
6 M. Sevik, The Response of a Propulsor to Random Velocity Fluctuations, in, 1970.
7 C.W. Jiang, M.S. Chang, Y.N. Liu, the effect of turbulence ingestion on propeller broadband thrust, in, 1991.
8 S.M. Abu Sharkh, S.R. Turnock, G. Draper, Performance of a tip-driven electric thruster for unmanned underwater vehicles, in: Proceedings of the International Offshore and Polar Engineering Conference, 2001, pp. 321-324.
9 A.J. Dubas, N.W. Bressloff, S.M. Sharkh, Numerical modelling of rotor-stator interaction in rim driven thrusters, Ocean Engineering, 106 (2015) 281-288.
10 B.W. Song, Y.J. Wang, W.L. Tian, Open water performance comparison between hub-type and hubless rim driven thrusters based on CFD method, Ocean Engineering, 103 (2015) 55-63.
11 Q.M. Cao, F.W. Hong, D.H. Tang, F.L. Hu, L.Z. Lu, Prediction of loading distribution and hydrodynamic measurements for propeller blades in a rim driven thruster, Journal of Hydrodynamics, 24 (2012) 50-57.
12 J. Wojno, T. Mueller, W. Blake, Turbulence ingestion noise, part2: rotor aeroacoustic response to grid generated turbulence, AIAA Journal 40 (2002) 7.
13 W.R. Sears, Some aspects of non-stationary air foil theory and tis practical application, J. Aeron. Sci., 8 (1941).
14 S. Chu, S. Widnall, Lifting surface theory for a semi-infinite wind in oblique gust, AIAA Journal, 12 (1974) 7.
15 J.O. Hinze, Turbulence, an introduction to its mechanics and theory, McGraw-Hill, New York, 1995.